Mean Field Theory of the Phase Behavior of Ternary Block Copolymer–Homopolymer Blends

M. Banaszak and M. D. Whitmore*

Department of Physics, Memorial University of Newfoundland, St. John's, Newfoundland, Canada A1B 3X7

Received May 6, 1991; Revised Manuscript Received July 20, 1991

ABSTRACT: We have extended and applied the theory of polymer blends developed by Hong and Noolandi to the calculation of phase diagrams of ternary A-*b*-B/A/B copolymer/homopolymer blends which can undergo microphase and macrophase separation. The approach used a perturbative solution to the modified diffusion equation to calculate the polymer distribution functions and the free energy. For simplicity, we assumed that the microphase is lamellar and calculated the free energy up to fourth order. The main results are phase diagrams for a variety of model systems containing symmetric or asymmetric copolymers mixed with homopolymers of varying molecular weights and for a PS-*b*-PI/PS/PI mixture. We also compared induced microphase formation in ternary and binary blends. It is particularly interesting in blends containing asymmetric copolymers and/or A and B homopolymers having differing molecular weights.

1. Introduction

Block copolymers and block copolymer/homopolymer and block copolymer/solvent blends can exhibit a variety of morphologies and phase behavior and are under active experimental (e.g., refs 1–16) and theoretical (e.g., refs 17–33) investigation. Block copolymers can undergo an order–disorder transition, frequently referred to as microphase separation, and at least four ordered morphologies exist: layers, cylinders, spheres, and the bicontinuous "double-diamond" structure.[3,13] Blends in which block copolymers are a component can also phase separate in the usual sense, which can be called *macrophase* separation. The goal of this paper is to provide a contribution to the understanding of microphase and macrophase separation in ternary copolymer/homopolymer blends of the form A-*b*-B/A/B, e.g., PS-*b*-PI/PS/PI.

It is clear from earlier work that a complete first-principles treatment of these systems remains in the future. The mean field self-consistent theory of Helfand and co-workers[17–23] provides a detailed description of the microphases of copolymers in the strong-segregation limit, including the equilibrium morphologies. Complementing this for the weak-segregation regime is the theory of Leibler,[24] which uses a random-phase approximation[34] and a fourth-order expansion for the free energy. It describes the order–disorder transition for block copolymers and predicts a phase diagram for them, but with phase boundaries separating the different microphases which do not seem to accord with experience (e.g., ref 3). The extension of this theory to include fluctuation effects by Fredrickson and Helfand[27] indicates that such effects are important, but the predicted phase diagrams still exhibit apparently anomalous features. For copolymer/solvent blends, self-consistent calculations indicate that other higher order effects are also important. For example, the copolymer density profiles are cosine-like, and the amplitudes of the density variations are small, only over limited ranges.[29,33] As well, the calculations predict that the lamellar thickness in these blends scales faster with copolymer molecular weight in the weak-segregation regime than in the strong-segregation regime, in apparent agreement with recent measurements.[16] On the other hand, such a mean field theory does not explain the apparent stretching of the blocks near the microphase separation transition but in the homogeneous phase which was observed in the same experiments. Thus we conclude that a full treatment of these systems may require incorporating both fluctuation effects and the equivalent of fully self-consistent calculations over the full temperature–composition range.

In this paper we discuss the phase behavior of ternary copolymer/homopolymer blends on the basis of a mean field theory which employs the fourth-order expansion of the free energy of the microphase, an expansion which is given in terms of the local density of A monomers. The approach does not include fluctuation effects, numerical solutions to the self-consistent field equations, or equation of state effects. Because of these limitations, we made no attempt to discriminate between different morphologies (lamellae, cylinders, spheres). Instead we explicitly assumed the lamellar structure. This can be at least partly justified on the grounds that, except very near the order–disorder transition, the differences between the free energies of any two microphases are generally much smaller than the difference between the free energy of any microphase and the homogeneous phase. This approach is an extension of the earlier treatment of binary copolymer/homopolymer blends[31,32] and can be thought of as the simplest model of these systems which incorporates both microphase and macrophase separation. The calculations here complement the recent discussion of critical behavior in such blends by Broseta and Fredrickson, which was based on an extension of the Leibler RPA theory, using what corresponds to the second-order term in the free energy of the microphase.[28]

When modeling the blend we assumed that each phase is either a homogeneous mixture or an ordered microphase, but these are not the only possibilities. In particular, copolymer micelles can form within each homopolymer-rich phase, or the copolymers could migrate to interfaces between homopolymer domains. Using a model of micelle formation developed earlier, we have tried to identify and thereby avoid systems in which micelles form.[35] We also assumed, for those cases where macrophase separation occurs, that *at equilibrium* the bulk phases are large, the total interfacial area is accordingly small, and consequently only an insignificant fraction of the copolymers migrates to interfaces.

Section 2 of the paper, along with the Appendix, describes the theory and detailed formulas, and section 3 sample results. Given the limitations of the approach, as described above, these results cannot be considered

0024-9297/92/2225-0249$03.00/0

quantitatively reliable, but instead should be used as guides to understanding the systems and the phenomena that can occur. Section 4 summarizes.

2. Theory

2.1. General. In this section we derive the basic expressions we use for the free energy of the blend. The first part of the derivation follows closely that of Hong and Noolandi,[30,31] but with the incompressibility incorporated following Ohta and Kawasaki.[26] As well, we specialize to the case of A-*b*-B copolymer and A and B homopolymers and make explicit use of this in our final expression for the free energy of the microphase. The results reduce to those for binary A-*b*-B/A blends in the limit of vanishing homopolymer B volume fraction.

We consider a volume V containing $\tilde{N}_C$ copolymer molecules with block degrees of polymerization Z_{CA} and Z_{CB}, $\tilde{N}_{HA}$ homopolymer molecules of type A with degree of polymerization Z_{HA}, and $\tilde{N}_{HB}$ homopolymer molecules of type B with degree of polymerization Z_{HB}. We associate with each component p, p = HA, HB, CA, and CB, a Kuhn statistical length b_p and bulk density ρ_{0p} (monomers per unit volume), and we assume that the Kuhn lengths and bulk densities of each homopolymer component are the same as those of the corresponding block of the copolymers. Assuming the blend to be incompressible, the partition function can be written

$$\mathbf{Z} = \prod_{\kappa}^{C} \frac{Z_\kappa^{\tilde{N}_\kappa}}{\tilde{N}_\kappa!} \int \prod_{i=1}^{\tilde{N}_{HA}} d\mathbf{r}_i(\cdot)\, P_{HA}[\mathbf{r}_i(\cdot)] \prod_{j=1}^{\tilde{N}_{HB}} d\mathbf{r}_j(\cdot)\, P_{HB}[\mathbf{r}_j(\cdot)] \times \left[\int \prod_{k=1}^{\tilde{N}_C} d\mathbf{r}_{Ak}(\cdot)\, d\mathbf{r}_{Bk}(\cdot)\, P_{CA}[\mathbf{r}_{Ak}(\cdot)]\, P_{CB}[\mathbf{r}_{Bk}(\cdot)] \times \delta[\mathbf{r}_{Ak}(Z_{CA}) - \mathbf{r}_{Bk}(Z_{CB})] \right] \delta\left[1 - \sum_p \frac{\hat{\rho}_p(\cdot)}{\rho_{0p}} \right] \exp[-\beta \hat{V}] \quad (1)$$

where Z_κ is the contribution to the partition function from the kinetic energy of a molecule of type κ, κ = HA, HB, and C. Here, and throughout this paper, the "C" over a product (or summation) sign indicates that for that product (or summation), the copolymer is to be treated as a single component; otherwise the two blocks are to be treated as distinct. The four weight functions are assumed to be of the standard Wiener form

$$P_p[\mathbf{r}(\cdot)] \propto \exp\left[-\frac{3}{2b_p^2} \int_0^{Z_p} d\tau\, \dot{\mathbf{r}}(\tau)^2 \right] \quad (2)$$

and the four number densities are given by

$$\hat{\rho}_p(\mathbf{r}) = \hat{\rho}_p(\mathbf{r}, \{\mathbf{r}_{pi}(\tau)\}) = \sum_{i=1}^{\tilde{N}_p} \int_0^{Z_p} d\tau\, \delta(\mathbf{r} - \mathbf{r}_{pi}(\tau)) \quad (3)$$

The expression $\delta(1 - \sum_p \hat{\rho}_p(\cdot)/\rho_{0p})$ in eq 1 ensures incompressibility.

The interaction energy, $\hat{V}$, is a functional of the densities $\hat{\rho}_p(\mathbf{r})$. It is convenient to express it in units of $k_BT = \beta^{-1}$ and model it via two-body interactions, $W_{pp'}(\mathbf{r} - \mathbf{r}')$. Then using the identity

$$\delta\left[1 - \sum_p \frac{\hat{\rho}_p(\cdot)}{\rho_{0p}} \right] \exp[-\beta \hat{V}] = \int \left[\prod_p d\rho_p(\cdot)\, \delta[\rho_p(\cdot) - \hat{\rho}_p(\cdot)] \right] \delta\left[1 - \sum_{p'} \frac{\rho_{p'}(\cdot)}{\rho_{0p'}} \right] \exp[-W] \quad (4)$$

with

$$W(\{\rho_p(\cdot)\}) = \frac{1}{2} \sum_{pp'} \int d\mathbf{r}\, d\mathbf{r}'\, \rho_p(\mathbf{r})\, W_{pp'}(\mathbf{r} - \mathbf{r}')\, \rho_{p'}(\mathbf{r}') \quad (5)$$

and substituting integral representations of the delta functions appearing in eq 4, we can write the partition function, eq 1, as

$$\mathbf{Z} = \mathcal{N} \prod_{\kappa}^{C} \frac{Z_\kappa^{\tilde{N}_\kappa}}{\tilde{N}_\kappa!} \int \left[\prod_p d\rho_p(\cdot)\, d\omega_p(\cdot) \right] d\eta(\cdot)\, [\mathcal{Q}_C]^{\tilde{N}_C} \times [\mathcal{Q}_{HA}]^{\tilde{N}_{HA}} [\mathcal{Q}_{HB}]^{\tilde{N}_{HB}} \exp\left\{ \int d\mathbf{r}\, \eta(\mathbf{r}) \left[1 - \sum_p \frac{\rho_p(\mathbf{r})}{\rho_{0p}} \right] + \sum_p \int d\mathbf{r}\, \omega_p(\mathbf{r})\, \rho_p(\mathbf{r}) - W[\{\rho_p(\mathbf{r})\}] \right\} \quad (6)$$

where $\mathcal{N}$ is the normalization. For homopolymers (p = HA or HB)

$$[\mathcal{Q}_p]^{\tilde{N}_p} = \int \prod_{i=1}^{\tilde{N}_p} d\mathbf{r}_i(\cdot)\, P_p[\mathbf{r}_i(\cdot)] \exp\{-\int d\mathbf{r}\, \omega_p(\mathbf{r})\, \hat{\rho}_p(\mathbf{r})\} \quad (7)$$

where $\hat{\rho}_p(\mathbf{r})$ is related to the $\{\mathbf{r}_i(\cdot)\}$ by eq 3. Equation 7 implies

$$\mathcal{Q}_p = \int d\mathbf{r}(\cdot)\, P_p[\mathbf{r}(\cdot)] \exp\{-\int_0^{Z_p} \omega_p[\mathbf{r}(\tau)]\, d\tau\} \quad (8)$$

For copolymers

$$\mathcal{Q}_C = \int d\mathbf{r}_A(\cdot)\, d\mathbf{r}_B(\cdot)\, P_{CA}[\mathbf{r}_A(\cdot)]\, P_{CB}[\mathbf{r}_B(\cdot)]\, \delta[\mathbf{r}_A(Z_{CA}) - \mathbf{r}_B(Z_{CB})] \exp\{-\int_0^{Z_{CA}} \omega_{CA}[\mathbf{r}_A(\tau)]\, d\tau - \int_0^{Z_{CB}} \omega_{CB}[\mathbf{r}_B(\tau)]\, d\tau\} \quad (9)$$

These functionals can be expressed in terms of four propagators $Q_p(\mathbf{r}, \tau | \mathbf{r}')$, all of which satisfy modified diffusion equations.[30] Explicitly, they are given by

$$\mathcal{Q}_p = \int d\mathbf{r}\, d\mathbf{r}'\, Q_p(\mathbf{r}, Z_p | \mathbf{r}') \quad (10)$$

for homopolymers, p = HA, HB, and

$$\mathcal{Q}_C = \int d\mathbf{r}\, d\mathbf{r}'\, d\mathbf{r}''\, Q_{CA}(\mathbf{r}'', Z_{CA} | \mathbf{r})\, Q_{CB}(\mathbf{r}'', Z_{CB} | \mathbf{r}') \quad (11)$$

for copolymers.

Using Stirling's approximation, the partition function, eq 6, can be written

$$\mathbf{Z} = \mathcal{N} \int \prod_p d\rho_p(\cdot)\, d\omega_p(\cdot)\, d\eta(\cdot) \times \exp\{-\mathcal{F}_T[\{\rho_p(\cdot)\}, \{\omega_p(\cdot)\}, \eta(\cdot)]\} \quad (12)$$

where $\mathcal{F}_T$ is the free energy functional (in units of k_BT), given by

$$\mathcal{F}_T[\{\rho_p(\cdot)\}, \{\omega_p(\cdot)\}, \eta(\cdot)] = \mathcal{F}(\{\rho_p(\cdot)\}, \{\omega_p(\cdot)\}) + \mathcal{H}[\{\rho_p(\cdot)\}, \eta(\cdot)] \quad (13)$$

with

$$\mathcal{F}[\{\rho_p(\cdot)\}, \{\omega_p(\cdot)\}] = W[\{\rho_p(\cdot)\}] - \sum_p \int d\mathbf{r}\, \omega_p(\mathbf{r})\, \rho_p(\mathbf{r}) + \sum_\kappa^{C} \tilde{N}_\kappa \left(\ln \frac{\tilde{N}_\kappa}{Z_\kappa \mathcal{Q}_\kappa} - 1 \right) \quad (14)$$

and

$$\mathcal{H}[\{\rho_p(\cdot)\},\eta(\cdot)] = \int d\mathbf{r}\, \eta(\mathbf{r})\left(\sum_p \frac{\rho_p(\mathbf{r})}{\rho_{0p}} - 1\right) \quad (15)$$

We next need expressions for the thermal average density distribution of each component. Using the partition function, eq 1, we can express this for, e.g., homopolymer HA as

$$\langle\hat{\rho}_{HA}(\mathbf{r})\rangle = \frac{1}{\mathbf{Z}}\prod_\kappa^C \frac{\mathcal{Z}_\kappa^{\tilde{N}_\kappa}}{\tilde{N}_\kappa!}\int\prod_{i=1}^{\tilde{N}_{HA}} d\mathbf{r}_i(\cdot)\, P_{HA}[\mathbf{r}_i(\cdot)]\, \hat{\rho}_{HA}(\mathbf{r},\{\mathbf{r}_i(\cdot)\}) \times \int\prod_{j=1}^{\tilde{N}_{HB}} d\mathbf{r}_j(\cdot)\, P_{HB}[\mathbf{r}_j(\cdot)]\left[\int\prod_{k=1}^{\tilde{N}_C} d\mathbf{r}_{Ak}(\cdot) \times d\mathbf{r}_{Bk}(\cdot)\, P_{CA}[\mathbf{r}_{Ak}(\cdot)]\, P_{CB}[\mathbf{r}_{Bk}(\cdot)]\, \delta[\mathbf{r}_{Ak}(Z_{CA}) - \mathbf{r}_{Bk}(Z_{CB})]\right] \times \delta\left[1 - \sum_p \frac{\hat{\rho}_p(\cdot)}{\rho_{0p}}\right] \exp[-\beta\hat{V}] \quad (16)$$

The functional integrals here are the same as in the partition function, except for the presence of the $\hat{\rho}_{HA}(\mathbf{r},\{\mathbf{r}_i(\cdot)\})$. Therefore we can introduce changes of variables as we did for $\mathbf{Z}$. The only difference is that $[\mathcal{Q}_{HA}]^{\tilde{N}_{HA}}$ is replaced with

$$\int\prod_{i=1}^{\tilde{N}_{HA}} d\mathbf{r}_i(\cdot)\, P_{HA}[\mathbf{r}_i(\cdot)]\, \hat{\rho}_{HA}(\mathbf{r}) \times \exp[-\int d\mathbf{r}'\, \omega_{HA}(\mathbf{r}')\, \hat{\rho}_{HA}(\mathbf{r}')] \quad (17)$$

which, by differentiating eq 7, is seen to be equal to

$$-\frac{\delta}{\delta\omega_{HA}(\mathbf{r})}[\mathcal{Q}_{HA}]^{\tilde{N}_{HA}} \quad (18)$$

We thus have, for either homopolymer,

$$\langle\hat{\rho}_p(\mathbf{r})\rangle = -\frac{\mathcal{N}}{\mathbf{Z}}\int\left[\prod_{p'} d\rho_{p'}(\cdot)\, d\omega_{p'}(\cdot)\right] d\eta(\cdot)\, \frac{\tilde{N}_p}{\mathcal{Q}_p}\frac{\delta\mathcal{Q}_p}{\delta\omega_p(\mathbf{r})} \times \exp\{-\mathcal{F}_T[\{\rho_{p'}(\cdot)\},\{\omega_{p'}(\cdot)\},\eta(\cdot)]\} \quad (19)$$

In fact, all four densities can be expressed

$$\langle\hat{\rho}_p(\mathbf{r})\rangle = -\frac{\mathcal{N}}{\mathbf{Z}}\int\left[\prod_{p'} d\rho_{p'}(\cdot)\, d\omega_{p'}(\cdot)\right] d\eta(\cdot)\, \frac{\tilde{N}_\kappa}{\mathcal{Q}_\kappa}\frac{\delta\mathcal{Q}_\kappa}{\delta\omega_p(\mathbf{r})} \exp[-\mathcal{F}FF_T[\{\rho_{p'}(\cdot)\},\{\omega_{p'}(\cdot)\},\eta(\cdot)]] \quad (20)$$

where $\kappa = p$ if p = HA or HB, or $\kappa = C$ if p = CA or CB.

2.2. Mean Field Approximation. Exact evaluation of integrals such as eqs 12 and 20 is beyond our current capability. In this paper we use the saddle point method, approximating the free energy and thermal averages by their values at the saddle point of $\mathcal{F}_T$; eq 20 becomes

$$\langle\hat{\rho}_p(\mathbf{r})\rangle \to -\frac{\tilde{N}_\kappa}{\mathcal{Q}_\kappa}\frac{\delta\mathcal{Q}_\kappa}{\delta\omega_p(\mathbf{r})}\Big|_{sp} \quad (21)$$

To find the saddle point we need to minimize $\mathcal{F}_T$ with respect to each $\rho_p(\mathbf{r})$, $\omega_p(\mathbf{r})$, and $\eta(\mathbf{r})$ subject to the constraint of constant particle numbers

$$\int d\mathbf{r}\, \rho_p(\mathbf{r}) = N_p \quad (22)$$

This minimization yields

$$\frac{\delta W}{\delta\rho_p(\mathbf{r})} - \omega_p(\mathbf{r}) + \lambda_p + \frac{\eta(\mathbf{r})}{\rho_{0p}} = 0 \quad (23)$$

$$\rho_p(\mathbf{r}) + \frac{\tilde{N}_\kappa}{\mathcal{Q}_\kappa}\frac{\delta\mathcal{Q}_\kappa}{\delta\omega_p(\mathbf{r})} = 0 \quad (24)$$

$$\sum_p \frac{\rho_p(\mathbf{r})}{\rho_{0p}} = 1 \quad (25)$$

where the λ_p are the Lagrange multipliers associated with eq 22. According to eqs 21 and 24, the saddle point values of the $\rho_p(\mathbf{r})$ correspond to the ensemble averages $\langle\hat{\rho}_p(\mathbf{r})\rangle$. Equation 25, arising from the incompressibility, makes $\mathcal{H} = 0$ at the saddle point, and hence the saddle point approximation to the free energy is

$$F \to \mathcal{F}[\{\rho_p(\cdot)\},\{\omega_p(\cdot)\}]|_{sp} \quad (26)$$

We assume that all A–B interactions are the same, irrespective of whether the interacting monomers belong to homopolymers or copolymers. With this assumption, the interaction energy can be expressed

$$W[\{\rho_p(\cdot)\}] = \frac{1}{2}\sum_p W_{pp}\rho_{0p}N_p + U_{AB}\int d\mathbf{r}\, [\rho_{HA}(\mathbf{r}) + \rho_{CA}(\mathbf{r})][\rho_{HB}(\mathbf{r}) + \rho_{CB}(\mathbf{r})] \quad (27)$$

where W_{pp} and U_{AB} are integrals of the $W_{pp'}(\mathbf{r} - \mathbf{r}')$.[30] Writing out eq 23 explicitly for the two cases p = HA and CA

$$U_{AB}[\rho_{HB}(\mathbf{r}) + \rho_{CB}(\mathbf{r})] - \omega_{HA}(\mathbf{r}) + \lambda_{HA} + \frac{\eta(\mathbf{r})}{\rho_{0A}} = 0 \quad (28)$$

$$U_{AB}[\rho_{HB}(\mathbf{r}) + \rho_{CB}(\mathbf{r})] - \omega_{CA}(\mathbf{r}) + \lambda_{CA} + \frac{\eta(\mathbf{r})}{\rho_{0A}} = 0 \quad (29)$$

and subtracting eq 29 from eq 28, we find

$$\omega_{HA}(\mathbf{r}) - \lambda_{HA} = \omega_{CA}(\mathbf{r}) - \lambda_{CA} \quad (30)$$

However, the overall level of each potential $\omega_p(\mathbf{r})$ is arbitrary. For this paper it is convenient to choose them so that

$$\int d\mathbf{r}\, \omega_p(\mathbf{r}) = 0 \quad (31)$$

Integrating both sides of eq 30 and using eq 31, we obtain

$$\lambda_{HA} = \lambda_{CA} \quad (32)$$

Thus

$$\omega_{HA}(\mathbf{r}) = \omega_{CA}(\mathbf{r}) \equiv \omega_\alpha(\mathbf{r}) \quad (33)$$

Similarly

$$\omega_{HB}(\mathbf{r}) = \omega_{CB}(\mathbf{r}) \equiv \omega_\beta(\mathbf{r}) \quad (34)$$

Thus at the saddle point, we have two distinct potentials, $\omega_\alpha(\mathbf{r})$ and $\omega_\beta(\mathbf{r})$.

We next rescale the mean field potentials, Kuhn statistical lengths, and degrees of polymerization, in order to use the explicit solution to the diffusion equation developed by Hong and Noolandi:[31]

$$\hat{\omega}_p(\mathbf{r}) = \rho_{0p}\omega_p(\mathbf{r})/\rho_0$$

$$\hat{b}_p^2 = \rho_{0p}b_p^2/\rho_0$$

$$r_{HA} = \rho_0 Z_{HA}/\rho_{0A}, \quad r_{HB} = \rho_0 Z_{HB}/\rho_{0B} \quad (35)$$

$$r_{CA} = \rho_0 Z_{CA}/\rho_{0A}, \quad r_{CB} = \rho_0 Z_{CB}/\rho_{0B}$$

$$r_C = r_{CA} + r_{CB}$$

where ρ_0 is an arbitrary reference density. We also introduce the local and average volume fractions of each of the four components

$$\phi_p(\mathbf{r}) = \langle \hat{\rho}_p(\mathbf{r}) \rangle / \rho_{0p} \tag{36}$$

and

$$\bar{\phi}_p = N_p / V\rho_{0p} \tag{37}$$

as well as the overall copolymer volume fraction

$$\bar{\phi}_C = \bar{\phi}_{CA} + \bar{\phi}_{CB} \tag{38}$$

Equation 21 can be rewritten as

$$\phi_p(\mathbf{r}) = -V\frac{\bar{\phi}_p}{r_p}\frac{\delta}{\delta\hat{\omega}_p(\mathbf{r})}\ln\frac{\mathcal{Q}_\kappa}{V}\bigg|_{sp} \tag{39}$$

With one final set of changes of variable, $\tau \rightarrow Z_p\tau$, the modified diffusion equation which the propagators satisfy is

$$\left[-\frac{b_p^2}{6}\nabla^2 + \hat{\omega}_p(\mathbf{r})\right] Q_p(\mathbf{r},\tau|\mathbf{r}') = -\frac{1}{r_p}\frac{\partial}{\partial\tau}Q_p(\mathbf{r},\tau|\mathbf{r}') \tag{40}$$

They satisfy the initial condition

$$Q_p(\mathbf{r},0|\mathbf{r}') = \delta(\mathbf{r}-\mathbf{r}') \tag{41}$$

We next use these results to calculate the saddle point approximation for the free energy, eq 14, which we can write as

$$F = F_{hom} + \Delta F \tag{42}$$

where F_{hom} is the free energy of a homogeneous bulk phase of the A-*b*-B/A/B blend and ΔF is due to inhomogeneities. For the homogeneous phase $\hat{\omega}_p(\mathbf{r}) = 0$, in which case eqs 40 and 41 are easily solved, with the result that $\mathcal{Q}_\kappa = V$ for all κ. Thus

$$F_{hom} = \frac{1}{2}\sum_p W_{pp}\rho_{0p}N_p + \rho_{0A}\rho_{0B}U_{AB}[\bar{\phi}_{HA} + \bar{\phi}_{CA}][\bar{\phi}_{HB} + \bar{\phi}_{CB}] + \sum_\kappa^C \tilde{N}_\kappa\left(\ln\frac{\tilde{N}_\kappa}{Z_\kappa V} - 1\right) \tag{43}$$

We can subtract from this the free energy of a fully demixed system, F_{ref}. Dividing by the total volume V and the reference density ρ_0 used above, we are left with the free energy density of a uniform, homogeneous blend relative to fully demixed, homogeneous systems:

$$f_{hom} \equiv \frac{F_{hom} - F_{ref}}{V\rho_0} = \sum_\kappa^C \frac{\bar{\phi}_\kappa}{r_\kappa}\ln\bar{\phi}_\kappa + \chi\bar{\phi}_\alpha\bar{\phi}_\beta \tag{44}$$

Here we have identified $U_{AB}\rho_{0A}\rho_{0B}/\rho_0$ as the Flory interaction parameter χ,[30] and $\bar{\phi}_\alpha$ and $\bar{\phi}_\beta$ are the average volume fractions of A and B in the system, $\bar{\phi}_\alpha = \bar{\phi}_{CA} + \bar{\phi}_{HA}$ and $\bar{\phi}_\beta = \bar{\phi}_{CB} + \bar{\phi}_{HB}$.

The remaining free energy density is that of a microphase-separated system relative to the homogeneous blend. For this, it is convenient to work with Fourier transforms of $\phi_p(\mathbf{r})$, $\hat{\omega}_p(\mathbf{r})$, and $Q_p(\mathbf{r},\tau|\mathbf{r}')$, which we label $\tilde{\phi}_p(\mathbf{k})$, $\tilde{\omega}_p(\mathbf{k})$, and $\tilde{Q}_p(\mathbf{k},\tau|\mathbf{k}')$. Equation 39 can be transformed to

$$\tilde{\phi}_p(\mathbf{k}) = -\frac{\bar{\phi}_p}{r_p}\frac{\delta}{\delta\tilde{\omega}_p(-\mathbf{k})}\ln\frac{\mathcal{Q}_\kappa}{V} \quad \text{for all } \mathbf{k} \neq 0 \tag{45}$$

With this, Δf can be written:

$$\Delta f \equiv \frac{\Delta F}{V\rho_0} = \frac{1}{V}\int' \frac{d\mathbf{k}}{(2\pi)^3}\chi[\tilde{\phi}_{HA}(\mathbf{k}) + \tilde{\phi}_{CA}(\mathbf{k})][\tilde{\phi}_{HB}(-\mathbf{k}) + \tilde{\phi}_{CB}(-\mathbf{k})] - \frac{1}{V}\int' \frac{d\mathbf{k}}{(2\pi)^3}\sum_p \tilde{\phi}_p(\mathbf{k})\tilde{\omega}_p(-\mathbf{k}) - \sum_\kappa^C \frac{\bar{\phi}_\kappa}{r_\kappa}\ln\frac{\mathcal{Q}_\kappa}{V} \tag{46}$$

and the "prime" on the integration symbol means to exclude $\mathbf{k} = 0$. Introduce the local volume fractions of A and B at each point:

$$\phi_\alpha(\mathbf{r}) = \phi_{HA}(\mathbf{r}) + \phi_{CA}(\mathbf{r}) \tag{47}$$

and

$$\phi_\beta(\mathbf{r}) = \phi_{HB}(\mathbf{r}) + \phi_{CB}(\mathbf{r}) \tag{48}$$

which, because of incompressibility, satisfy $\phi_\alpha(\mathbf{r}) + \phi_\beta(\mathbf{r}) = 1$. In Fourier space they satisfy

$$\tilde{\phi}_\beta(\mathbf{k}) = -\tilde{\phi}_\alpha(\mathbf{k}) \quad \text{for } \mathbf{k} \neq 0 \tag{49}$$

Equation 46 can now be transformed to

$$\Delta f = \frac{1}{V}\int' \frac{d\mathbf{k}}{(2\pi)^3}\chi\tilde{\phi}_\alpha(\mathbf{k})\,\tilde{\phi}_\beta(-\mathbf{k}) - \frac{1}{V}\int' \frac{d\mathbf{k}}{(2\pi)^3}\sum_p \tilde{\phi}_p(\mathbf{k})\,\tilde{\omega}_p(-\mathbf{k}) - \sum_\kappa^C \frac{\bar{\phi}_\kappa}{r_\kappa}\ln\frac{\mathcal{Q}_\kappa}{V} \tag{50}$$

2.3. Fourth-Order Expansion. At this point we further approximate our expressions, invoking a perturbative solution to the diffusion equation.[31] For any potential $\tilde{\omega}_p(\mathbf{k})$, $\tilde{Q}_p(\mathbf{k},\tau|\mathbf{k}')$ can be given as an expansion in the $\tilde{\omega}_p$, which can be integrated as in eqs 10 and 11 to yield

$$\frac{\mathcal{Q}_\kappa}{V} = 1 + \frac{(-r_\kappa)^2}{2!V}g^\kappa_{ij}\tilde{\omega}_i\tilde{\omega}_j + \frac{(-r_\kappa)^3}{3!V}g^\kappa_{ijk}\tilde{\omega}_i\tilde{\omega}_j\tilde{\omega}_k + \frac{(-r_\kappa)^4}{4!V}g^\kappa_{ijkl}\tilde{\omega}_i\tilde{\omega}_j\tilde{\omega}_k\tilde{\omega}_l + \dots \tag{51}$$

where $i \equiv (i,k_i)$, $\tilde{\omega}_i = \tilde{\omega}_i(-\mathbf{k})$, and summation over subscript and integration over wavevector are implied by repeated indices. The functions $g^\kappa_{ij\dots l}$ are given in ref 31 and the Appendix.

Using eq 51 in an expansion of the last term of eq 50 and further simplifying by using $\tilde{\omega}_\alpha$ and $\tilde{\omega}_\beta$ in place of ω_{HA}, etc., Δf can be expressed

$$\Delta f = \frac{1}{V}\int' \frac{d\mathbf{k}}{(2\pi)^3}\chi\tilde{\phi}_\alpha(\mathbf{k})\,\tilde{\phi}_\beta(\mathbf{k}) - \frac{1}{V}\int' \frac{d\mathbf{k}}{(2\pi)^3}[\tilde{\phi}_\alpha(\mathbf{k})\,\tilde{\omega}_\alpha(-\mathbf{k}) + \tilde{\phi}_\beta(\mathbf{k})\,\tilde{\omega}_\beta(-\mathbf{k})] - \frac{1}{2V}\mathcal{G}_{ij}\tilde{\omega}_i\tilde{\omega}_j + \frac{1}{6V}\mathcal{G}_{ijk}\tilde{\omega}_i\tilde{\omega}_j\tilde{\omega}_k - \frac{1}{24V}\mathcal{G}_{ijkl}\tilde{\omega}_i\tilde{\omega}_j\tilde{\omega}_k\tilde{\omega}_l \tag{52}$$

with the detailed coefficients given in the Appendix.

We next need comparable expansions for the thermal average density distributions, eq 21 or 45. Since eq 51 is valid for any potential, it can be differentiated as indicated in eq 45, and then the derivatives can be evaluated at the saddle point. This results in expressions for the four $\tilde{\phi}_p$, given in terms of the two potentials $\tilde{\omega}_\alpha$ and $\tilde{\omega}_\beta$. Adding pairs of these expressions as indicated in eqs 47 and 48

yields, for $\mathbf{k} \neq 0$

$$\tilde{\phi}_i(\mathbf{k}) = -\mathcal{G}_{ij}\tilde{\omega}_j + \frac{1}{2}\mathcal{G}_{ijk}\tilde{\omega}_j\tilde{\omega}_k - \frac{1}{6}\mathcal{G}_{ijkl}\tilde{\omega}_j\tilde{\omega}_k\tilde{\omega}_l \quad (53)$$

for $i,j,k,l = \alpha$ or β, and the $\mathcal{G}$'s are the same as in eq 52. This could be substituted into eq 52, and the resulting expression for Δf minimized with respect to the potentials. However, it is convenient to first invert eq 53. Up to third order, and for $\mathbf{k} \neq 0$, this yields

$$\tilde{\omega}_i(\mathbf{k}) = \Gamma^2_{ij}\tilde{\phi}_j + \Gamma^3_{ijk}\tilde{\phi}_j\tilde{\phi}_k + \Gamma^4_{ijkl}\tilde{\phi}_j\tilde{\phi}_k\tilde{\phi}_l \quad (54)$$

where the Γ's are given in the Appendix. Substituting eq 54 into eq 52 and using eq 49, we have

$$\Delta f = \sum_{\mathbf{k}_1}{}' f^{(2)}(\mathbf{k}_1,-\mathbf{k}_1)\,\tilde{\phi}_\alpha(\mathbf{k}_1)\,\tilde{\phi}_\alpha(-\mathbf{k}_1) + \sum_{\mathbf{k}_1,\mathbf{k}_2}{}' f^{(3)}(\mathbf{k}_1,\mathbf{k}_2,-\mathbf{k}_1-\mathbf{k}_2)\,\tilde{\phi}_\alpha(\mathbf{k}_1)\,\tilde{\phi}_\alpha(\mathbf{k}_2)\,\tilde{\phi}_\alpha(-\mathbf{k}_1-\mathbf{k}_2) + \sum_{\mathbf{k}_1,\mathbf{k}_2,\mathbf{k}_3}{}' f^{(4)}(\mathbf{k}_1,\mathbf{k}_2,\mathbf{k}_3,-\mathbf{k}_1-\mathbf{k}_2-\mathbf{k}_3)\,\tilde{\phi}_\alpha(\mathbf{k}_1) \times \tilde{\phi}_\alpha(\mathbf{k}_2)\,\tilde{\phi}_\alpha(\mathbf{k}_3)\,\tilde{\phi}_\alpha(-\mathbf{k}_1-\mathbf{k}_2-\mathbf{k}_3) \quad (55)$$

where the prime on the sums means to exclude $\mathbf{k}_i = 0$. The coefficients $f^{(2)}$, $f^{(3)}$, and $f^{(4)}$ are listed in the Appendix.

2.4. Calculation of Phase Diagrams. In this paper we calculate phase diagrams of these systems in the weak-segregation regime, assuming a lamellar structure for the microphase. To do so, for each system we first calculate the free energy per unit volume for all compositions, $\bar{\phi}_{HA}$, $\bar{\phi}_{HB}$, and $\bar{\phi}_C$, including Δf if so indicated. Because we are treating the weak-segregation regime, for the purposes of calculating Δf we approximate $\phi_\alpha(x)$ by the simple circular function[24,28]

$$\phi_\alpha(x) = \bar{\phi}_\alpha + \bar{\psi}_\alpha \cos(kx) \quad (56)$$

and of course $\phi_\beta(x) = 1 - \phi_\alpha(x)$. The second term in eq 56 models the variation of $\phi_\alpha(x)$ about its mean value, with $\bar{\psi}_\alpha$ being the amplitude of this variation. Away from the order–disorder transition, other wavenumbers must be included to calculate the density profiles, repeat distances, etc.,[33] but in this paper we make no attempt to calculate these other quantities.

A consequence of using eq 56 and assuming the lamellar structure is that only wavevectors of magnitude k appear in the summations of eq 55, and furthermore the third-order term vanishes. The remaining sums for $f^{(2)}$ and $f^{(4)}$ are independent of $\bar{\psi}_\alpha$ and result in an expression of the form

$$\Delta f = A(k)\bar{\psi}_\alpha^{\,2} + B(k)\bar{\psi}_\alpha^{\,4} \quad (57)$$

The next step is to locate the minimum of $A(k)$, say at k^*. If $A(k^*) > 0$ then it indicates that the homogeneous phase is stable relative to the microphase, and the free energy density for that blend is $f = f_{hom}$. However, if $A(k^*) < 0$ then it indicates that the microphase is stable relative to the homogeneous mixture. In this case we evaluate $B(k^*)$ and minimize eq 57 by calculating $\bar{\psi}_\alpha = [-A(k^*)/2B(k^*)]^{1/2}$, giving

$$\Delta f = -\frac{A(k^*)^2}{4B(k^*)} \quad (58)$$

The resulting (negative) value for Δf is then added to the Flory–Huggins free energy f_{hom}, to give the free energy density of a single phase at that composition.

This produces a full free energy surface for the system. From this surface we next locate order–disorder transition lines, where $A(k^*) = 0$, and the spinodals for macrophase separation, where, e.g.

$$\begin{vmatrix} \frac{\partial^2}{\partial\phi_{HA}^{\,2}}f & \frac{\partial^2}{\partial\phi_{HA}\partial\phi_{HB}}f \\ \frac{\partial^2}{\partial\phi_{HB}\partial\phi_{HA}}f & \frac{\partial^2}{\partial\phi_{HB}^{\,2}}f \end{vmatrix} = 0 \quad (59)$$

Having located the spinodals, the next step is finding the tie lines and binodals. Two phases coexist at points 1 and 2 of the phase diagram if there exists a plane which is tangent to the free energy surface at those two points but which lies below it everywhere else.[36] Such a pair of points is connected by a tie line, and the locus of these pairs of points constitutes binodal lines. If there is a plane which is tangent to the free energy surface at three different points but which lies below it elsewhere, then these three points enclose a three-phase region. In this paper we consider two- and three-phase regions.

Our numerical procedure for finding the tangent planes is based on that of Hsu and Prausnitz[37] and consists of minimizing a convenient function of three (for a two-phase region) or six (for a three-phase region) variables.

3. Results

3.1. Symmetric Model Systems. Even for ternary systems which do not undergo an order–disorder transition, e.g., those described by a simple Flory–Huggins model for the free energy, there is a multitude of possible phase diagram topologies.[38] In this paper we consider some of the interesting possibilities for systems which undergo both microphase and macrophase separation. For reasons identified above, we limit the discussion to the weak-segregation regime but reemphasize that even here the results should be considered primarily as guides to the behavior which can occur.

We begin with model system calculations for which all reference densities and Kuhn lengths are taken to be equal. For purposes of illustration, we choose copolymers with $Z_C = 400$. Perfectly symmetric copolymers with this value of Z_C microphase separate at $\chi Z_C = 10.5$, or $\chi \simeq 0.0263$ (in this level of approximation), and this sets the overall scale of the values of χ used here. The other important system characteristics are the composition of the copolymers, i.e., Z_{CA}/Z_C, and the degrees of polymerization of each homopolymer relative to the copolymers.

The value of χ depends at least on temperature and in general on degrees of polymerization and concentrations as well. However, in this paper, for each blend we neglect its dependence on overall concentrations and do not need to relate it directly to either temperature or degrees of polymerization.

Our first three sets of calculations are for what we call a symmetric system, containing copolymers with $Z_{CA} = Z_{CB} = Z_C/2$ and homopolymers with equal degrees of polymerization, $Z_{HA} = Z_{HB} \equiv Z_H$. Figure 1 shows four phase diagrams for the case of relatively low homopolymer molecular weight, $Z_H = Z_C/8$, which is $Z_H = 50$ in this case. For $\chi Z_C < 10.5$ (not shown) the system is in a single homogeneous phase for all compositions. As χ is increased beyond this value, e.g., the temperature is lowered, the first feature which appears is microphase separation of the pure copolymer. This is illustrated in the first panel of Figure 1, for which $\chi Z_C = 12$. Addition of these low molecular weight homopolymers in any proportion tends to dissolve the microphase, but there is no macrophase separation anywhere on the diagram. (In principle, there is a small two-phase region between the M and H regions which vanishes in this approach.) Thus there are only a single microphase region, M, and a single homogeneous

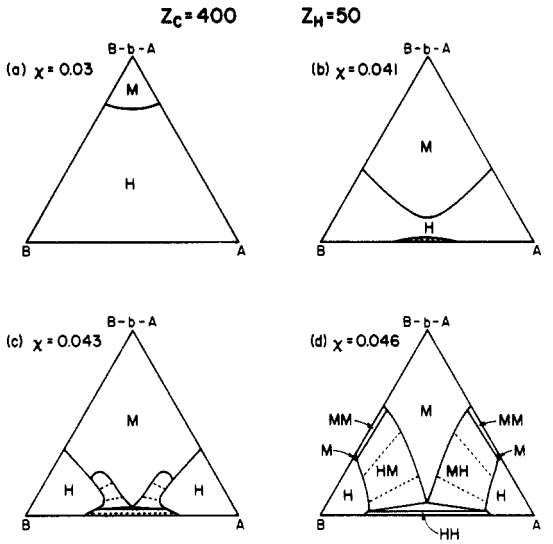

Figure 1. Calculated phase diagrams for a model symmetric ternary A-*b*-B/A/B blend with copolymer degree of polymerization Z_C = 400 (Z_{CA} = Z_{CB} = Z_C/2), homopolymer degrees of polymerization Z_{HA} = Z_{HB} = 50, and four values of the Flory interaction parameter as indicated. All reference volumes ρ_{0p} and Kuhn statistical lengths b_p are taken to be equal. In each of these diagrams, the apex of the triangle represents pure copolymers, and each of the other vertices represents pure A or B homopolymers. Each edge represents a binary blend, and each interior point represents a ternary blend. Regions where a single homogeneous phase is stable are labeled H, and those where a single microphase is stable are labeled M. Two-phase regions are indicated by explicit labels, such as HH or MH, and/or by the presence of the straight tie lines. In these cases the two coexisting phases are indicated by the two phases in which the tie lines terminate. There is a triangular three-phase region in each of panels c and d (very small in panel c), bounded by 3 two-phase regions.

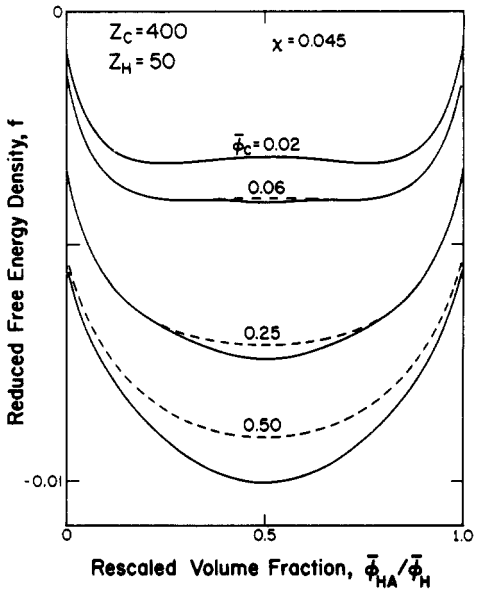

Figure 2. Slices of the free energy surface as a function of homopolymer A content for the blend of Figure 1 with χ = 0.045 and different copolymer volume fractions $\bar{\phi}_C$ as indicated. In each case, the solid line is the full free energy density, the dashed line is f_{hom}, and the difference is Δf. For each curve the horizontal axis is rescaled by a factor equal to the total homopolymer content, $\bar{\phi}_H$ = $\bar{\phi}_{HA}$ + $\bar{\phi}_{HB}$.

phase region, H, on this diagram. As the value of χ is further increased up to the point where χZ_H = 2, the only change is an increase in size of the M region. Beyond this, the binary homopolymer blend phase separates, creating a two-phase HH region near the base of the phase diagram. The second panel of Figure 1 corresponds to the case where this has begun. It is also apparent from this panel that the microphase is relatively stable near the isopleth, i.e, along the vertical line on the phase diagram from the apex of the triangle to the base, along which the overall A:B composition ratio is 50:50. Along the isopleth, in this case the microphase persists to copolymer volume fractions as low as about 15%. By contrast, in each binary copolymer/homopolymer blend it persists only to about 40% copolymer content. With a further increase in χ, the regions of microphase and macrophase separation overlap, as indicated in the third panel of Figure 1, for which χ = 0.043. At this point the phase diagram has become quite rich, exhibiting single-phase M and H regions, a two-phase HH region at the base of the triangle, two-phase MH "fingers", and a very small three-phase region. (It also indicates tiny two-phase MM regions at the tip of each "finger", but the reliability of such details is almost certainly beyond the capabilities of the current approach.) In the final panel of Figure 1, χ is further increased so that the binary copolymer/homopolymer blends macrophase separate. For each such binary blend, there is an MM region, but it gives way to an MH region if there is even a small amount of the other homopolymer present. It should also be pointed out that there is probably even further structure to these diagrams because of the possibility of other morphologies.

Perhaps the most interesting feature of Figure 1 is the predicted relative stability of the single M phase near the isopleth. It persists to very large homopolymer content but is destabilized by disparate amounts of A and B homopolymers. This result is consistent with the experimental finding of Tanaka et al.[8] for PS-*b*-PI/PS/PI blends, who found the long-range order persisting to copolymer volume fractions as low as $\bar{\phi}_C$ = 0.1. The behavior can be understood physically by considering horizontal "slices" of the free energy surface, shown in Figure 2 which is for χ = 0.045, which corresponds qualitatively to panel c of Figure 1. These slices do not represent the phase separation quantitatively, because not all the tie lines are horizontal, but they illustrate the controlling features. The top curve shows the free energy for near-zero copolymer content, $\bar{\phi}_C$ = 0.02, which corresponds to a horizontal line very near to the base of the associated phase diagram. There is a region of negative curvature near the center of this curve, which causes macrophase separation to two homogeneous phases, consistent with Figure 1c or 1d. In this case the binodal points correspond to the two minima in the free energy. The other sets of curves, which correspond to progressively more copolymer content, illustrate that there is a competition between the Flory–Huggins free energy of mixing which tends to induce macrophase separation and the free energy of the microphase which tends to stabilize the microphase, with maximum effect near the isopleth. For very small copolymer content, Δf is too small to have an effect and the system continues to separate to two homogeneous phases. However, further increasing the copolymer content, the second set of curves, both increases the magnitude of Δf at the center and reduces the tendency toward macrophase separation. This stabilizes the microphase near the isopleth, but there are still unstable regions on either side of the central minimum, which induce macrophase separation. Following this curve across from left to right would indicate a sequence of phases of H → HM → M → MH → H. This corresponds qualitatively to horizontally traversing Figure 1c or 1d from a single H region, through an HM "finger", through the central M region, and so on to the other side. With a further increase in copolymer content, the third set of curves, the regions of negative curvature shrink and then disappear, implying a sequence H → M → H, and the

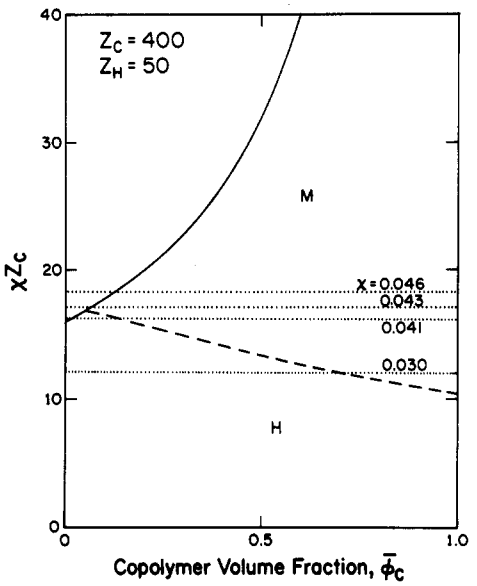

Figure 3. Stability limits for the macrophase (—) and microphase (– – –) transitions for the copolymer/homopolymer blend used in Figures 1 and 2, along the isopleth. The horizontal lines correspond to the values of χ used in Figure 1.

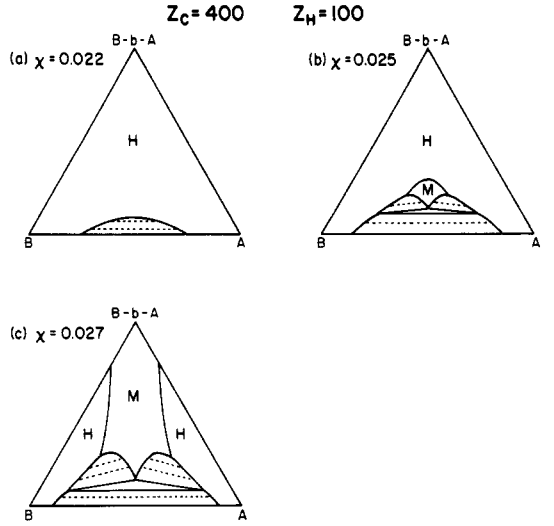

Figure 4. Calculated phase diagrams for a model symmetric A-*b*-B/A/B blend for a copolymer with $Z_C = 400$ as in Figure 1, homopolymer degrees of polymerization increased to $Z_{HA} = Z_{HB} = 100$, and three values of χ as indicated. The notation is as in Figure 1.

microphase persists over more of the "slice". This corresponds qualitatively to a traverse of Figure 1c, passing just above the MH "fingers". Finally, for large enough copolymer content, the last set of curves, the microphase M persists over the entire slice, as in the uppermost regions of Figures 1c and 1d.

Figure 3 gives a complementary perspective on this system, showing the stability limits for macrophase and microphase separation[5,8,39] along the isopleth, i.e., $\bar{\phi}_{HA} = \bar{\phi}_{HB}$, with $\bar{\phi}_C$ varying from 0 to 1. The horizontal lines indicate the values of χ used in Figure 1. The slopes of the phase boundaries, both of which are monotonic in this case, indicate that these copolymers tend to stabilize microphase separation but reduce the tendency toward macrophase separation. Moving down the isopleth from the apex to the base of the triangle of Figure 1a corresponds to moving from right to left along the lower horizontal line of Figure 3. In both cases, the phase changes from M to H at $\bar{\phi}_C \simeq 0.7$. Moving down the isopleth in Figure 1b corresponds to moving along the second line in Figure 3, with the sequence of phases M → H → HH. Finally, the isopleths in Figures 1c and 1d correspond to the two top lines of Figure 3, with the implied sequence of phases being M to a macrophase-separated system, without an intervening single-phase H region.

Figure 4 is for a system which is the same as that discussed in Figures 1–3 except that the homopolymer degrees of polymerization are increased to $Z_H = Z_C/4$, so that the molecular weight of each homopolymer is one-half that of the corresponding block of the copolymer. In this case, for $\chi < 0.02$ there is no structure to the phase diagram. As χ is increased, the first feature to appear is the macrophase separation of the two homopolymers; the first panel shows this for $\chi = 0.022$. The next panel is for the case $\chi = 0.025$, for which $\chi Z_C = 10$, and so the copolymer does not microphase separate. Furthermore, adding *either* A or B homopolymers to the copolymer (binary blends) induces neither microphase nor macrophase separation. This is consistent with earlier results for binary systems.[32] However, addition of A *and* B homopolymers in nearly equal proportions, i.e., near the isopleth, induces both, resulting in a new feature for the phase diagram. Starting at the top of the isopleth, adding homopolymers induces microphase separation at about 70% homopolymer. Further additional homopolymer induces macrophase separation, and in this region of the phase diagram there are two-phase MH regions as well as a three-phase region. Below this is an HH region. Larger values of χ increase the tendencies toward both kinds of phase separation. Figure 4c is for the case in which it is increased slightly, enough so that the neat copolymer microphase separates but not enough to induce binary copolymer/homopolymer blends to macrophase separate.

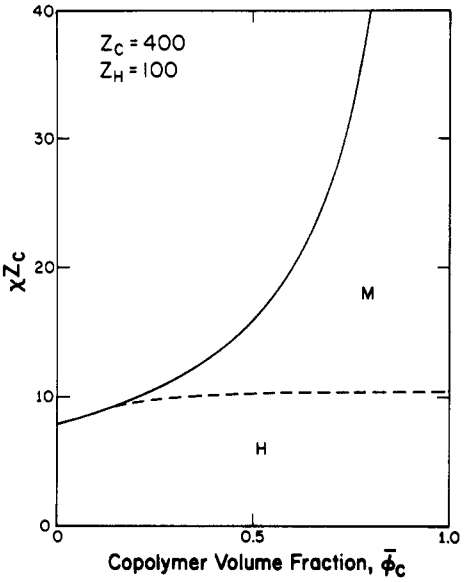

Figure 5. Stability limits for the macrophase (—) and microphase (– – –) transitions for the copolymer/homopolymer blend used in Figure 4, along the isopleth.

As illustrated in Figure 5, for this system the two stability limits along the isopleth are again both monotonic, but this time their slopes have the same sign. For larger values of Z_H/Z_C (not shown) the slopes of both lines increase in magnitude. The case illustrated is, in fact, very near the one in which the microphase stability limit is nearly horizontal as $\bar{\phi}_C \to 1$. A horizontal boundary in this limit would imply that small amounts of homopolymer tend to neither stabilize nor destabilize the microphase. This implies in turn that, as for binary copolymer/homopolymer blends,[32] there is a threshold such that if Z_H exceeds this threshold, then small amounts of homopolymer tend

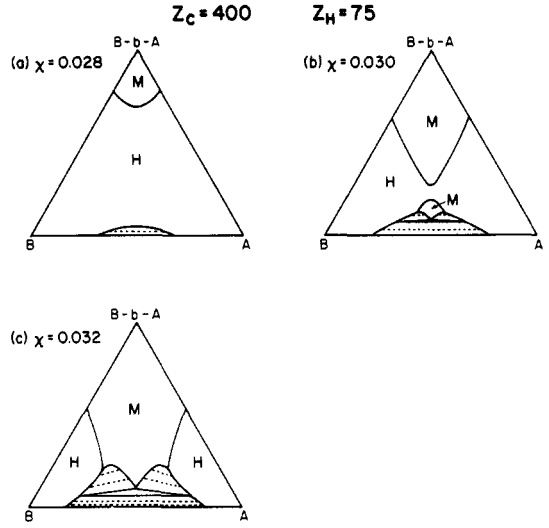

Figure 6. Calculated phase diagrams for a model symmetric A-*b*-B/A/B blend for copolymer with $Z_C = 400$ as in Figure 1, homopolymer degrees of polymerization $Z_{HA} = Z_{HB} = 75$, and three values of χ as indicated. The notation is as in Figure 1.

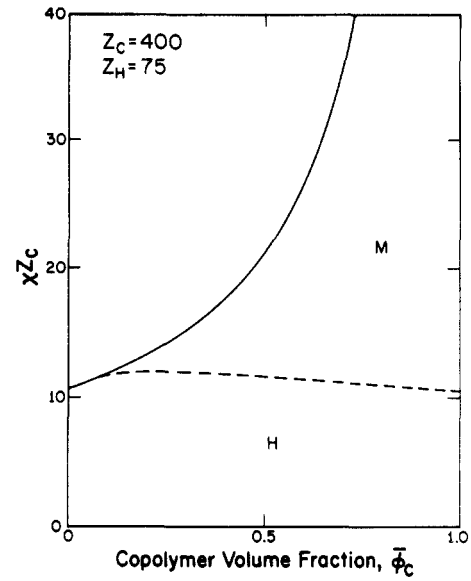

Figure 7. Stability limits for the macrophase (—) and microphase (- - -) transitions for the copolymer/homopolymer blend used in Figure 6, along the isopleth.

to induce microphase separation, but lower molecular weight homopolymers tend to destabilize it. In both cases, for these model systems with symmetric copolymers, we find that this threshold is very close to $Z_H = Z_C/4$.

Finally, Figure 6 contains phase diagrams for the intermediate case $Z_H = 75 \simeq Z_C/5.3$. In this case, for $\chi \lesssim 0.0263$ the phase diagram is featureless. Copolymer microphase separation and homopolymer macrophase separation both appear at $\chi \simeq 0.0265$, as illustrated in the first panel for which $\chi = 0.028$. In this case small amounts of these relatively low molecular weight homopolymers tend to destabilize the microphase. However, as seen in Figure 6b, the theory predicts a new effect for this system. Although small amounts of homopolymer destabilize the microphase, additional homopolymer can then restabilize it. The sequence of phases along the isopleth is M → H → M → macrophase separation. This is, however, a very delicate effect; a slight further increase in χ, such as to a value of 0.032 as in the last panel of this figure, causes it to disappear, and furthermore the phenomenon might well be eliminated by other effects such as a composition-dependent χ or fluctuation effects.

The predicted existence of two distinct M regions in Figure 6b can be related to the stability limits, shown in Figure 7. The important point is that the stability limit of the microphase in this case is nonmonotonic. Initially, addition of homopolymer destabilizes the microphase, but this tendency reaches a maximum near $\bar{\phi}_C \simeq 0.2$ and for greater amounts of homopolymer this phase boundary turns downward for a short interval before macrophase separation occurs.

This phenomenon could also be explored by small-angle X-ray scattering (SAXS) from the homogeneous phase.[9,24] The intensity of such scattering is proportional to the inverse of the coefficient of the second term in the free energy expansion, $f^{(2)}$ of eq 55. The scattering from a fully symmetric system with compositions which place it on the isopleth can be expressed[40]

$$I(\mathbf{k}) \propto \left[\frac{S(k)}{W(k)} - 2\chi\right]^{-1} \tag{60}$$

where k is the magnitude of the scattering vector, and

$$\frac{S(k)}{W(k)} = \left[\bar{\phi}_C \frac{r_C}{8}[g^{(2)}_{CA}(\mathbf{k},-\mathbf{k}) - g^{(1)}_{CA}(\mathbf{k})^2] + \bar{\phi}_H \frac{r_H}{4} g^{(2)}_H(\mathbf{k},-\mathbf{k})\right]^{-1} \tag{61}$$

where $\bar{\phi}_H$ is the total homopolymer volume fraction and $g^{(2)}_H$ could refer to either homopolymer. For the special case $\chi = 0$, this reduces to

$$I(\mathbf{k}) \propto \bar{\phi}_C \frac{r_C}{8}[g^{(2)}_{CA}(\mathbf{k},-\mathbf{k}) - g^{(1)}_{CA}(\mathbf{k})^2] + \bar{\phi}_H \frac{r_H}{4} g^{(2)}_H(\mathbf{k},-\mathbf{k}) \tag{62}$$

There are two terms in eq 62, proportional to the copolymer and homopolymer volume fractions, respectively. The first peaks at a finite wavenumber, whereas the second peaks at $k = 0$. In general, as homopolymer is substituted for copolymer, the peak in $I(k)$ moves toward zero wavenumber, but the value at maximum can either increase, which signals the case in which the homopolymer tends to stabilize the microphase, or decrease, which signals the homopolymer tending to destabilize it.

The scattering profiles for $\chi = 0$, i.e., eq 62, for the system used in Figures 6 and 7 are shown in Figure 8. They are presented as a function of $R_g k$, where R_g is the unperturbed radius of gyration of the copolymers, $R_g^2 = Z_C b^2/6$. The first panel is for pure copolymer; the peak occurs at $R_g k^* = 1.95$, which is equivalent to $Z_C(k^* b)^2 = 22.7$, and has the value $I(k^*) = Z_C/21$. The second panel is for $\bar{\phi}_C = 0.5$, which shows the copolymer and homopolymer contributions as well as the total. The resultant peak has moved toward $k = 0$ and in this case has decreased in value. This is consistent with Figures 6 and 7, in which addition of homopolymer initially destabilizes the microphase. The third panel, which is for $\bar{\phi}_C = 0.2$, is similar. However, for the case $\bar{\phi}_C = 0.15$, shown in the last panel, the peak value has increased slightly, consistent with the reappearance of the M-phase region in Figure 6b.

3.2. Asymmetric Model Systems. We consider next two model systems in which the reference densities and Kuhn lengths are again equal but the degrees of polymerization are not. In the first, we use symmetric copolymers but choose different homopolymers, $Z_{HA} \neq Z_{HB}$, and in the second case choose asymmetric copolymers but $Z_{HA} = Z_{HB}$.

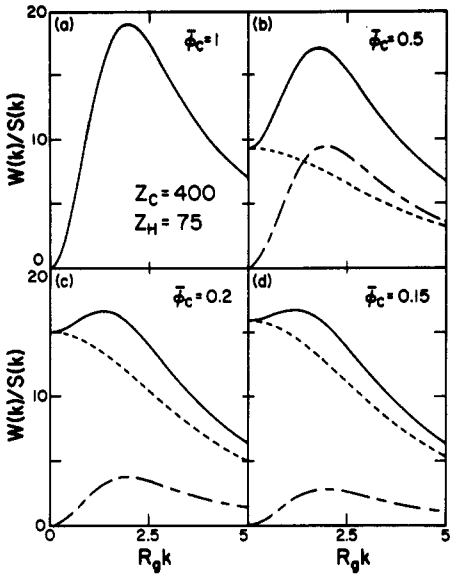

Figure 8. Calculated scattering curves for the ternary system of Figures 6 and 7 for four different compositions $\bar{\phi}_C$ as indicated, along the isopleth. Each figure shows the total curve (—), the contribution proportional to $\bar{\phi}_C$ (– – –), and the contribution proportional to ϕ_H (- - -).

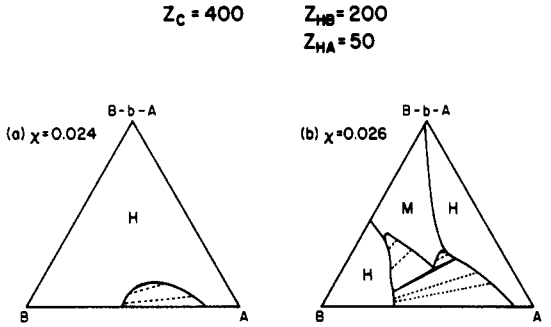

Figure 9. Calculated phase diagrams for a model A-*b*-B/A/B blend with a symmetric copolymer with Z_C = 400 as in Figures 1–8 but with homopolymer degrees of polymerization Z_{HA} = 50 and Z_{HB} = 200 and two values of χ as indicated. The notation is as in Figure 1.

Figure 9 shows phase diagrams for the symmetric copolymer, Z_C = 400, but Z_{HA} = 50 and Z_{HB} = 200. In this case the first feature to appear is homopolymer phase separation, occurring for $\chi \geq 0.0225$; the first panel of Figure 9 is for $\chi = 0.024$, where this phase separation is seen. Increasing the value of χ to 0.026 produces the diagram of the second panel. In this case $\chi Z_C = 10.4$, just below the threshold for pure copolymer microphase separation. Addition of the relatively high molecular weight B homopolymer (binary blend) induces microphase separation but not macrophase separation, whereas the relatively low molecular weight A homopolymer induces neither. In the ternary blend, both types of phase separation occur.

The relative stability of the single M phase appears here as well. In this case it falls primarily within the region of the phase diagram where there is more homopolymer B than homopolymer A, corresponding to an overall excess of B type monomer in the system. This is consistent with the tendencies of the relatively high molecular weight B homopolymers to stabilize the microphase and the low molecular weight A homopolymers to destabilize it.

Figure 10 shows calculated phase diagrams for a system with Z_{CA} = 240 and Z_{CB} = 160 and $Z_{HA} = Z_{HB} = Z_H = 50$ as in Figure 1. The effects of asymmetry in the copolymer can be observed by comparing Figure 10 with Figure 1. In this case, the copolymer composition is 40:60 and so is

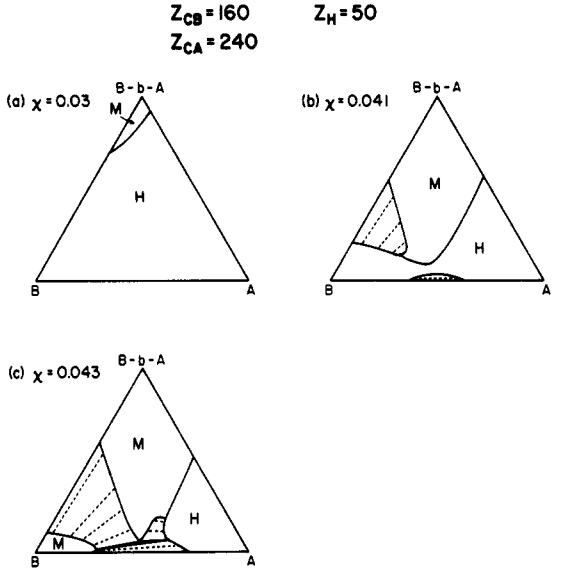

Figure 10. Calculated phase diagrams for a model A-*b*-B/A/B blend with Z_C = 400 as in Figures 1–9 but with asymmetric copolymers with Z_{CA} = 240 and Z_{CB} = 160 and homopolymer degrees of polymerization $Z_{HA} = Z_{HB}$ = 50. The three panels correspond to three values of χ as indicated. The notation is as in Figure 1.

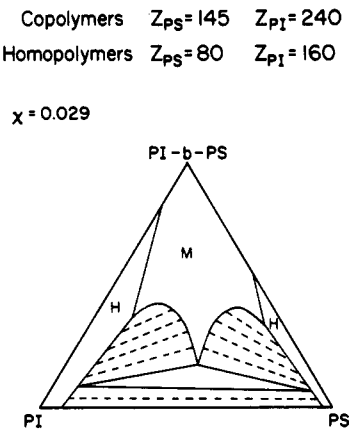

Figure 11. Calculated phase diagram for PS-*b*-PI/PS/PI, using measured values of the Kuhn statistical lengths and monomer volumes, degrees of polymerization as indicated, and $\chi = 0.029$.

probably very close to the lamellae–cylinders boundary. The first feature to appear is copolymer microphase separation, occurring for $\chi \geq 0.0284$; the first panel is for $\chi = 0.030$. Both homopolymers tend to destabilize the microphase, but the A homopolymer sooner than the B homopolymer. This is reasonable since additional A homopolymers drive the overall composition ratio even further from 50:50, whereas additional B homopolymers drive it toward 50:50. Increasing the value of χ to 0.039 causes the binary copolymer/B homopolymer blend to phase separate, and then at $\chi = 0.04$ the homopolymers also phase separate. Both these features are present in the second panel of Figure 10, for which $\chi = 0.041$. With further increases in χ, the phase-separated regions further overlap, resulting in an asymmetric phase diagram such as that of the third panel, for which $\chi = 0.043$.

3.3. Real Systems: Polystyrene/Polyisoprene. As a final application, Figure 11 shows a calculated phase diagram for a ternary PS-*b*-PI/PS/PI mixture. These copolymers and copolymer blends have been studied extensively experimentally, for example, by Hashimoto and co-workers.[1-9] For this calculation, we specified the copolymers to have Z_{PS} = 145 and Z_{PI} = 240, corresponding to samples used in a number of experiments.[3,5,7-9] The

volume fractions for the neat copolymer system are $\bar{\phi}_{PS} \simeq 0.45$ and $\bar{\phi}_{PI} \simeq 0.55$. To obtain an interesting phase diagram, for the homopolymers we chose $Z_{H,PS} = 80$ and $Z_{H,PI} = 160$, which are about 55% and 66% of the corresponding blocks of the copolymers.

We also used independently determined Kuhn statistical lengths and reference densities:[4,41]

$$b_A = 0.68 \text{ nm} \qquad \rho_{0A} = 6.07 \text{ nm}^{-3} \tag{63}$$

for styrene and

$$b_B = 0.59 \text{ nm} \qquad \rho_{0B} = 8.07 \text{ nm}^{-3} \tag{64}$$

for isoprene. Finally, to keep the entire blend in the weak-segregation regime, we chose $\chi = 0.029$, which is close to measured values for neat copolymers (especially to the "effective" interaction parameters for systems diluted with nonselective solvent).[9]

As seen in the figure, for these choices the theory indicates that the pure copolymer is microphase separated. Addition of either homopolymer PI or PS dissolves the microphase, but more PS (about 50%) than PI (about 15%) is required. This is consistent with the fact that as homopolymer PS is initially added to the copolymer, the overall PS:PI composition ratio changes from 45:55 toward 50:50, an effect which would tend to stabilize the microphase relative to the homogeneous phase. However, it is perhaps surprising because the homopolymer PS has the lower molecular weight, both in absolute terms and relative to the corresponding copolymer block, which would of itself indicate that the PS would have the greater tendency to destabilize the microphase. The actual behavior is governed by a competition between these two effects.

The binary homopolymer blend exhibits macrophase separation, but neither one of the binary copolymer/homopolymer blends does. For the ternary blends, the single phase is predicted to be relatively stable near the isopleth, as in the earlier cases. In fact, the topology of this diagram is most like that of Figure 4c; the differences are due primarily to the asymmetry of the components.

The persistence of the single microphase to very low copolymer content is consistent with the experimental result of Tanaka et al.,[8] who used these copolymers but lower molecular weight homopolymers. A full quantitative theoretical–experimental comparison would require performing similar calculations using appropriate homopolymer degrees of polymerization and values of χ, which would place the pure copolymer system outside the weak-segregation regime.

4. Summary

We have extended and applied the mean field formalism developed by Hong and Noolandi to calculate phase diagrams for ternary A-*b*-B/A/B copolymer/homopolymer blends in the weak-segregation regime. The method calculates the polymer distribution functions via perturbative solutions to the modified diffusion equations, and these are used to express the free energy density as an expansion in terms of the local density of A (or alternatively B) monomers, with contributions from both homopolymers and copolymers. The microphase separation transition was approximated as the condition for the homogeneous phase to be unstable relative to the lamellar microphase. This approach does not include fluctuation effects,[27] numerical solutions to the self-consistent-field equations,[29,33] or equation of state effects. Because of these limitations, we made no attempt to discriminate between different morphologies (lamellae, cylinders, spheres). Instead we explicitly assumed the lamellar structure and restricted our attention to systems in which the copolymer block degrees of polymerization Z_{CA} and Z_{CB} were chosen so that A and B volume fractions in each copolymer satisfied $f_A \simeq f_B \simeq 0.5$. Even for these systems there is probably more structure to these diagrams than we exhibit due to the existence of other morphologies throughout the phase diagram. The approach can be thought of as the simplest treatment of these systems which incorporates microphase and macrophase separation, and the results should be considered primarily as guides to behavior which can occur. The method is a modification of earlier treatments of binary copolymer/homopolymer blends.[31,32]

When modeling the blend we assumed that each phase is either homogeneous or an ordered microphase. We used a model of micelle formation developed earlier to identify and thereby avoid systems in which disordered micellar phases form,[35] and we assumed that at equilibrium only an insignificant fraction of the copolymers migrates to interfaces (for those cases where macrophase separation occurs).

Most of our results were presented as phase diagrams for symmetric and asymmetric model systems in which we chose the Kuhn statistical lengths and the monomer volumes to be equal for all components. We found that even for simple systems a variety of topologies occurs. One feature which appeared in a number of cases, and which is consistent with at least one set of experiments,[8] is the relative stability of the microphase for blends with overall A:B compositions near 50:50. This was particularly noticeable for those cases in which both microphase and macrophase separation occurred.

We also examined the phenomenon of induced microphase formation. For a fully symmetric model system, $Z_{CA} = Z_{CB} \equiv Z_C/2$, $Z_{HA} = Z_{HB} \equiv Z_H$, a small amount of homopolymer tends to stabilize a microphase in the ternary blend under the same conditions as in the binary blend, i.e., if $Z_H \geq Z_C/4$. However, the theory predicted two additional effects. First, for some cases homopolymers can induce the microphase in the ternary blend when they do not in either corresponding binary blend; i.e., an M region appears near the center of the phase diagram. Second, homopolymers of relatively low molecular weight, namely that for $Z_H \simeq Z_C/5.3$, tend to first destabilize the microphase and then to restabilize it. This phenomenon would likely be very hard to observe directly, but it might be possible to explore it using small-angle X-ray scattering from the homogeneous phase.

We also considered model systems in which the reference densities and Kuhn lengths were equal, as before, but the degrees of polymerization were not. In one case we used symmetric copolymers mixed with homopolymers which had unequal degrees of polymerization, and in the other we used asymmetric copolymers mixed with homopolymers with equal degrees of polymerization. We ended with a calculation for PS-*b*-PI/PS/PI, using appropriate monomer volumes and Kuhn statistical lengths and a reasonable value for the interaction parameter. Such calculations allow one to explore some of the competition between the effects of overall A:B concentrations and individual degrees of polymerization on the compatibility and morphologies of these blends. For example, in the case studied, addition of homopolymer PI had more of a tendency to destabilize the microphase than did additionof homopolymer PS, despite the fact that it had the higher molecular weight.

Acknowledgment. We thank Drs. J. M. Coombes, T. Hashimoto, and J. P. Whitehead for helpful discussions and Mr. J. Vavasour for help with the numerical work.

This work was supported in part by the Natural Sciences and Engineering Research Council of Canada.

Appendix: Expansion Coefficients

This Appendix lists the coefficients needed in section 2. Throughout, repeated indices imply summation and integration over wavevector.

The first expansion in the text is for $\mathcal{Q}_\kappa/V$, eq 51, which involves the $g^\kappa_{i...j}$. These are given explicitly in ref 31; here we reproduce their form. For homopolymer, κ = HA or HB, $g^\kappa_{i...j}$ is nonzero only if $i = ... = j = \kappa$, in which case

$$g^\kappa_{i...j} = (2\pi)^3\delta(\mathbf{k}_i + ... + \mathbf{k}_j)g^{(n)}_\kappa(\mathbf{k}_i,...,\mathbf{k}_j) \tag{65}$$

For copolymers, κ = C, then $i,...,j$ must be either CA or CB, and then

$$g^{\mathrm{C}}_{i...j} = (2\pi)^3\delta(\mathbf{k}_i + ... + \mathbf{k}_j)f_{\mathrm{A}}{}^m f_{\mathrm{B}}{}^{n-m}g^{(m)}_{\mathrm{CA}}(\mathbf{k}_i + ... + \mathbf{k}_l) \times g^{(n-m)}_{\mathrm{CB}}(\mathbf{k}_p + ... + \mathbf{k}_j) \tag{66}$$

where $\kappa_i = ... = \kappa_l$ = A, m subscripts, $\kappa_p = ... = \kappa_j$, $(n - m)$ subscripts, and $f_{\mathrm{A}} = r_{\mathrm{CA}}/r_{\mathrm{C}}$, $f_{\mathrm{B}} = r_{\mathrm{CB}}/r_{\mathrm{C}}$ (see eq 35). The functions $g^{(n)}_\kappa$ of eqs 65 and 66 are given in ref 31.

In the next expansion, eq 52, $i,j,... = \alpha$ or β. Each term can be written as a sum of homopolymer and copolymer contributions:

$$\mathcal{G}_{ij} = r_{\mathrm{HP}}\bar{\phi}_{\mathrm{HP}}g^{\mathrm{HP}}_{ij} + r_{\mathrm{C}}\bar{\phi}_{\mathrm{C}}g^{\mathrm{C}}_{ij} \tag{67}$$

$$\mathcal{G}_{ijk} = r^2_{\mathrm{HP}}\bar{\phi}_{\mathrm{HP}}g^{\mathrm{HP}}_{ijk} + r^2_{\mathrm{C}}\bar{\phi}_{\mathrm{C}}g^{\mathrm{C}}_{ijk} \tag{68}$$

$$\mathcal{G}_{ijkl} = r^3_{\mathrm{HP}}\bar{\phi}_{\mathrm{HP}}\left(g^{\mathrm{HP}}_{ijkl} - \frac{3}{V}g^{\mathrm{HP}}_{ij}g^{\mathrm{HP}}_{kl}\delta_{ik}\right) + r^3_{\mathrm{C}}\bar{\phi}_{\mathrm{C}}\left(g^{\mathrm{C}}_{ijkl} - \frac{3}{V}g^{\mathrm{C}}_{ij}g^{\mathrm{C}}_{kl}\right) \tag{69}$$

with i, j, k, and $l = \alpha$ or β, and HP denotes the homopolymer indicated by i, e.g.

$$g^{\mathrm{HP}}_{ij} = \delta_{i,\alpha}g^{\mathrm{HA}}_{ij} + \delta_{i,\beta}g^{\mathrm{HB}}_{ij} \tag{70}$$

$$r_{\mathrm{HP}}\bar{\phi}_{\mathrm{HP}}g^{\mathrm{HP}}_{ij} = \delta_{i,\alpha}r_{\mathrm{HA}}\bar{\phi}_{\mathrm{HA}}g^{\mathrm{HA}}_{ij} + \delta_{i,\beta}r_{\mathrm{HB}}\bar{\phi}_{\mathrm{HB}}g^{\mathrm{HB}}_{ij} \tag{71}$$

etc.. The $\mathcal{G}$'s are also used in eq 53.

The coefficients of eq 54, which arise from inverting eq 53, involve the inverses of the $\mathcal{G}$'s:

$$\Gamma_{ij} = -[\mathcal{G}]^{-1}_{ij} \tag{72}$$

$$\Gamma_{ijk} = \frac{1}{2}[\mathcal{G}]^{-1}_{is}[\mathcal{G}]^{-1}_{jp}[\mathcal{G}]^{-1}_{kq}\mathcal{G}_{spq} \tag{73}$$

$$\Gamma_{ijkl} = \frac{1}{2}[\mathcal{G}]^{-1}_{ip}[\mathcal{G}]^{-1}_{jq}\mathcal{G}_{pqs}[\mathcal{G}]^{-1}_{sr}\mathcal{G}_{rvt}[\mathcal{G}]^{-1}_{vk}[\mathcal{G}]^{-1}_{tl} - \frac{1}{6}[\mathcal{G}]^{-1}_{ip}[\mathcal{G}]^{-1}_{jv}[\mathcal{G}]^{-1}_{ks}[\mathcal{G}]^{-1}_{lt}\mathcal{G}_{pvst} \tag{74}$$

For the final expression for the free energy, eq 55, it is convenient to introduce first the related quantities $\hat{\gamma}^{(n)}_{ij...}$. We list the four second-order ones explicitly and the rest more generally:

$$\hat{\gamma}^{(2)}_{\alpha\alpha}(\mathbf{k}_1,-\mathbf{k}_1) = \frac{1}{2}[\mathcal{G}]^{-1}_{\alpha\alpha}(\mathbf{k}_1,-\mathbf{k}_1) \tag{75}$$

$$\hat{\gamma}^{(2)}_{\alpha\beta}(\mathbf{k}_1,-\mathbf{k}_1) = \hat{\gamma}^{(2)}_{\beta\alpha}(\mathbf{k}_1,-\mathbf{k}_1) = \frac{1}{2}(\chi + [\mathcal{G}]^{-1}_{\alpha\beta}(\mathbf{k}_1,-\mathbf{k}_1)) \tag{76}$$

$$\hat{\gamma}^{(2)}_{\beta\beta}(\mathbf{k}_1,-\mathbf{k}_1) = \frac{1}{2}[\mathcal{G}]^{-1}_{\beta\beta}(\mathbf{k}_1,-\mathbf{k}_1) \tag{77}$$

$$\hat{\gamma}^{(3)}_{ijk}(\mathbf{k}_1,\mathbf{k}_2,\mathbf{k}_3) = -\frac{1}{6}\sum_{spq}[\mathcal{G}]^{-1}_{is}(\mathbf{k}_1,-\mathbf{k}_1) \times [\mathcal{G}]^{-1}_{jp}(\mathbf{k}_2,-\mathbf{k}_2)[\mathcal{G}]^{-1}_{kq}(\mathbf{k}_3,-\mathbf{k}_3)\mathcal{G}_{spq}(\mathbf{k}_1,\mathbf{k}_2,\mathbf{k}_3) \tag{78}$$

$$\hat{\gamma}^{(4)}_{ijkl}(\mathbf{k}_1,\mathbf{k}_2,\mathbf{k}_3,\mathbf{k}_4) = -\frac{1}{24}\sum_{spqt}[\mathcal{G}]^{-1}_{is}(\mathbf{k}_1,-\mathbf{k}_1)[\mathcal{G}]^{-1}_{jp}(\mathbf{k}_2,-\mathbf{k}_2)[\mathcal{G}]^{-1}_{kq}(\mathbf{k}_3,-\mathbf{k}_3) \times [\mathcal{G}]^{-1}_{lt}(\mathbf{k}_4,-\mathbf{k}_4)\mathcal{G}_{spqt}(\mathbf{k}_1,\mathbf{k}_2,\mathbf{k}_3,\mathbf{k}_4) + \frac{1}{8}\sum_{pqsrvt}[\mathcal{G}]^{-1}_{ip}(\mathbf{k}_1,-\mathbf{k}_1) \times [\mathcal{G}]^{-1}_{jq}(\mathbf{k}_2,-\mathbf{k}_2)\mathcal{G}_{pqs}(\mathbf{k}_1,\mathbf{k}_2,-\mathbf{k}_1-\mathbf{k}_2)[\mathcal{G}]^{-1}_{sr}(\mathbf{k}_1+\mathbf{k}_2,-\mathbf{k}_1-\mathbf{k}_2) \times \mathcal{G}_{rvt}(\mathbf{k}_1+\mathbf{k}_2,\mathbf{k}_3,\mathbf{k}_4)[\mathcal{G}]^{-1}_{vk}(\mathbf{k}_3,-\mathbf{k}_3)[\mathcal{G}]^{-1}_{tl}(\mathbf{k}_4,-\mathbf{k}_4) \tag{79}$$

Defining

$$\Delta_i = \begin{cases} 1 & \text{if } i = \alpha \\ -1 & \text{if } i = \beta \end{cases} \tag{80}$$

then

$$f^{(2)}(\mathbf{k}_1,-\mathbf{k}_1) = \sum_{ij}\hat{\gamma}^{(2)}_{ij}(\mathbf{k}_1,-\mathbf{k}_1)\Delta_i\Delta_j \tag{81}$$

$$f^{(3)}(\mathbf{k}_1,\mathbf{k}_2,\mathbf{k}_3) = \sum_{ijk}\hat{\gamma}^{(3)}_{ijk}(\mathbf{k}_1,\mathbf{k}_2,\mathbf{k}_3)\Delta_i\Delta_j\Delta_k \tag{82}$$

$$f^{(4)}(\mathbf{k}_1,\mathbf{k}_2,\mathbf{k}_3,\mathbf{k}_4) = \sum_{ijkl}\hat{\gamma}^{(4)}_{ijkl}(\mathbf{k}_1,\mathbf{k}_2,\mathbf{k}_3,\mathbf{k}_4)\Delta_i\Delta_j\Delta_k\Delta_l \tag{83}$$

References and Notes

(1) Inoue, T.; Soen, T.; Hashimoto, T.; Kawai, H. *Macromolecules* **1970**, *3*, 87.
(2) Hashimoto, H.; Fujimura, M.; Hashimoto, T.; Kawai, H. *Macromolecules* **1981**, *14*, 844.
(3) Hasegawa, H.; Tanaka, H.; Yamasaki, K.; Hashimoto, T. *Macromolecules* **1987**, *20*, 1651.
(4) Mori, K.; Tanaka, H.; Hasegawa, H.; Hashimoto, T. *Polymer* **1989**, *30*, 1389.
(5) Hashimoto, T.; Tanaka, H.; Iizuka, N. In *Space–Time Organization in Macromolecular Fluids* (Springer Series in Chemical Physics); Tanaka, F., Doi, M., Ohta, T., Ed.; Springer-Verlag: Berlin, 1989; Vol. 51.
(6) Koizumi, S.; Hasegawa, H.; Hashimoto, T. *Macromolecules* **1990**, *23*, 2955.
(7) Hashimoto, T.; Tanaka, T.; Hasegawa, H. *Macromolecules* **1990**, *23*, 4378.
(8) Tanaka, H.; Hasegawa, H.; Hashimoto, T. *Macromolecules* **1991**, *24*, 240.
(9) Tanaka, H.; Hashimoto, T. *Macromolecules*, submitted.
(10) Owens, J. N. Ph.D. Thesis, Princeton University, 1986.
(11) Quan, X.; Gancarz, I.; Koberstein, J. T.; Wignall, G. D. *Macromolecules* **1987**, *20*, 1431.
(12) Koberstein, J. T.; Russell, T. P.; Walsh, D. J.; Pottick, L. *Macromolecules* **1990**, *23*, 877.
(13) Thomas, E. L.; Alward, D. B.; Kinning, D. L.; Martin, D. L.; Handlin, D. L., Jr.; Fetters, L. J. *Macromolecules* **1986**, *19*, 2197.
(14) Kinning, D. J.; Winey, K. I.; Thomas, E. L. *Macromolecules* **1988**, *21*, 3502.
(15) Winey, K. I. Ph.D. Thesis, University of Massachusetts, 1991.
(16) Almdal, K.; Rosedale, J. H.; Bates, F. S.; Wignall, G. D.; Fredrickson, G. H. *Phys. Rev. Lett.* **1990**, *65*, 1112.
(17) Helfand, E. In *Recent Advances in Polymer Blends, Grafts and Blocks*; Sperling, L. H., Ed.; Plenum: New York, 1974.
(18) Helfand, E. *Macromolecules* **1975**, *8*, 552.
(19) Helfand, E. *J. Chem. Phys.* **1975**, *62*, 999.
(20) Helfand, E.; Wassermann, Z. R. *Macromolecules* **1976**, *9*, 879.
(21) Helfand, E.; Wassermann, Z. R. *Macromolecules* **1978**, *11*, 960.
(22) Helfand, E.; Wassermann, Z. R. *Macromolecules* **1980**, *13*, 994.
(23) Helfand, E.; Wassermann, Z. R. In *Developments in Block Copolymers*; Goodman, I., Ed.; Elsevier: New York, 1982; Vol. 1.
(24) Leibler, L. *Macromolecules* **1980**, *13*, 1602.
(25) Leibler, L. *Makromol. Chem., Rapid Commun.* **1981**, *2*, 393.
(26) Ohta, T.; Kawasaki, K. *Macromolecules* **1986**, *19*, 2621.
(27) Fredrickson, G. H.; Helfand, E. *J. Chem. Phys.* **1987**, *87*, 697.
(28) Broseta, D.; Fredrickson, G. H. *J. Chem. Phys.* **1990**, *93*, 2927.
(29) Noolandi, J.; Hong, K. M. *Ferroelectrics* **1980**, *30*, 117.
(30) Hong, K. M.; Noolandi, J. *Macromolecules* **1981**, *14*, 727.
(31) Hong, K. M.; Noolandi, J. *Macromolecules* **1983**, *16*, 1083.
(32) Whitmore, M. D.; Noolandi, J. *Macromolecules* **1985**, *18*, 2486.
(33) Whitmore, M. D.; Noolandi, J. *J. Chem. Phys.* **1990**, *93*, 2946.
(34) de Gennes, P.-G. *Scaling Concepts in Polymer Physics*; Cornell University Press: Ithaca, NY, 1979.
(35) Whitmore, M. D.; Noolandi, J. *Macromolecules* **1985**, *18*, 657.

(36) Furman, S.; Dattagupta, S.; Griffiths, R. B. *Phys. Rev. B* **1977**, *15*, 441.
(37) Hsu, C. C.; Prausnitz, J. M. *Macromolecules* **1974**, *7*, 320.
(38) Knobler, C. M.; Scott, R. L. In *Phase Transitions and Critical Phenomena*; Domb, C., Lebowitz, J. L., Eds.; Academic Press: London, 1984; Vol. 9.
(39) Tanaka, H.; Hashimoto, T. *Polymer* **1988**, *29*, 212.
(40) Tanaka, H.; Sakurai, S.; Hashimoto, T.; Whitmore, M. D. *Polymer*, in press.
(41) Brandrup, J.; Immergut, E. H., Eds. *Polymer Handbook*, 2nd ed.; Interscience: New York, 1975.
(42) Bonner, C. C.; Prausnitz, J. M. *AIChE J.* **1973**, *19*, 943.
(43) Höcker, H.; Blake, C. J.; Flory, P. J. *Trans. Faraday Soc.* **1971**, *67*, 2251.

Registry No. (PI)(PS) (block copolymer), 105729-79-1; PS (homopolymer), 9003-53-6; PI (homopolymer), 9003-31-0.